Computational Condensed Matter 45 (2025) e01122

Contents lists available at ScienceDirect

Computational Condensed Matter

journal homepage: www.elsevier.com/locate/cocom

Reproducible density functional theory predictions of bandgaps for materials

Chenxi Lu [a], Musen Li [a,b,c], Michael J. Ford [c], Rika Kobayashi [d], Roger D. Amos [e], Jeffrey R. Reimers [a,c,*]

[a] International Centre for Quantum and Molecular Structures and Department of Physics, Shanghai University, Shanghai, 200444, China
[b] School of Materials Science and Engineering & Materials Genome Institute, Shanghai University, Shanghai, 200444, China
[c] University of Technology Sydney, School of Mathematical and Physical Sciences, Ultimo, New South Wales, 2007, Australia
[d] ANU Supercomputer Facility, Leonard Huxley Bldg. 56, Mills Rd, Canberra, ACT, 2601, Australia
[e] University of New South Wales Canberra, Canberra, ACT, 2600, Australia

A B S T R A C T

Even though reproducible computational procedures for density-functional-theory (DFT) calculations of molecular properties are well established, the additional complexities for calculations of materials properties present significant current issues. Considering a randomly selected set of 340 3D materials, we demonstrate that standard computational protocols lead to c. a. 20 % occurrences of significant failures during bandgap calculations. The bandgap is a quintessential materials property that underpins the prediction of most other properties. Examined herein are the effects of the choice of the pseudopotential to describe core electrons, the plane-wave basis-set cutoff energy, and the Brillouin-zone integration. For the pseudopotential and the cutoff energy, optimization of internal computational parameters is performed. For the Brillouin-zone integration, a new computational protocol is developed that chooses grids by minimization of interpolation errors using the second-derivative matrix of the orbital energies. This is shown to provide significant enhancement over established procedures that seek merely to maximize integration-grid densities.

1. Introduction

Three dimensional materials have attracted extensive research owing to their interesting photon properties [1], and have extremely broad application prospects in fields such as displays [1] and energy-storage batteries [2]. A material's bandgap influences both the highest wavelength at which it absorbs light and the energy that it can store. This then affects properties such as the efficiency of solar cells [3] and the transmission performance of optical fibers [4] with indeed materials with specific bandgaps being required in solar cells [5] and fiber optic sensors [6,7]. For semiconductors, a material's bandgap also influences its conductivity and usefulness [8]. In general, choosing a specific bandgap material directly affects the performance of the semiconductor device [9]. The reliable prediction of bandgaps is therefore a computation challenge of great value. A critical aspect for the determination of reliable results is the reproducible evaluation of properties, for each applied physical model, that are independent of the computational algorithms, protocols and internal parameters used.

The two most widely applied physical models for the prediction of bandgaps for materials are density functional theory [10,11] (DFT) and Green's Function (GW) theory [12]. These approaches are related, however, as GW approaches require a set of starting orbitals, and usually orbitals obtained from DFT are used. Typically, the results from the GW calculations are more reliable than their DFT counterparts, with GW often reaching the level of accuracy needed to make predictions of, e.g., spectroscopic transition energies and electrochemical potentials that are reliable enough for the interpretation of material's properties. Optimizing DFT calculations therefore is universally relevant.

Applications of DFT require the specification of the density functional, leading to the currently wide selection available for physical DFT models, and the reliability of each method for the prediction of experimental data varies considerably [13–15]. As representative examples of different classes of DFT models, we consider two density functionals: the generalized gradient approximation (GGA) functional designed by Perdew, Burke and Ernzerhof (PBE) [16], and that as modified to produce the PBE0 hybrid functional [17]. Hybrid functionals embed some contribution of Hartree-Fock terms to the exchange energy and required significantly more computational resources when implemented in

* Corresponding author. International Centre for Quantum and Molecular Structures and Department of Physics, Shanghai University, Shanghai, 200444, China.
E-mail addresses: MusenLi@shu.edu.cn (M. Li), Rika.Kobayashi@anu.edu.au (R. Kobayashi), R.Amos@unsw.edu.au (R.D. Amos), Jeffrey.Reimers@uts.edu.au (J.R. Reimers).

https://doi.org/10.1016/j.cocom.2025.e01122
Received 29 March 2025; Received in revised form 23 July 2025; Accepted 26 August 2025
Available online 28 August 2025

plane-wave codes such as those typically used to study materials. Concerning reliability, each density functional has its own sets of advantages and inadequacies. Often the treatment of self-interaction errors and partial occupancies presents significant issues [18], with models such as PBE and PBE0 that do not correct the asymptotic potential underestimating, to differing degrees, bandgaps, spectral transition energies, exciton binding strengths, and spectral assignment [19–23]. Typically, PBE0 predicts properties in better agreement with experiment than does PBE, but this feature is not of concern herein.

Owing to their intrinsically different properties, the PBE and PBE0 physical DFT models present different challenges for their reproducible evaluation. These aspects include both parameters used internally in a DFT calculation, and computational protocols that string together different DFT calculations to model the desired physical property. Considered are three aspects that are usually treated as internal parameters in DFT calculations: the pseudopotential (PP), the basis-set description, and the Brillouin-zone integration. We show that currently recommended procedures can be inadequate, and present optimized procedures for the PP and basis-set descriptions, as well as introducing a new computational protocol to guarantee reproducible Brillouin-zone integration. We focus not only on direct effects that these features have on calculations at the one material structure but also on the effect that they can have through induced structural changes.

In DFT calculations, PPs are used to represent core electrons. This can have a large effect in reducing computational demands. In addition, for heavy elements with inner-core electrons that experience strong relativistic effects, this procedure can remove the requirement for explicit treatment of spin-orbit interactions. Also, the exclusion of 1s electrons from explicit representation ensures that the electron density varies smoothly near the nucleus. In all-electron calculations, the electron-nucleus attraction is described by the standard Coulomb potential. In calculations using PPs, empirical potentials describe the interactions between the valence electrons and an unpolarizable system containing the nucleus and the core electrons. Different software packages performing calculations on materials often use PPs designed specifically for their own computational approach. For most atoms, software packages make a range of PPs available, differing by the number of electrons incorporated into the core and in the quality of their representation. Well-tuned PP and other computational parameters can facilitate the accurate prediction of properties of solids [24,25], while significantly reducing computational costs. We consider two PPs implemented in the VASP software package [26,27]: a standard one designed for efficient applications involving GGA-type density functionals such as PBE, and an enhanced one designed to give accurate results compatible with the increased accuracy that can be achieved using either GW methods and/or advanced density functionals [28].

The basis-sets available in most computational software packages designed for materials typically consist of plane waves that are truncated at some cutoff energy E_{cut}. Rapid changes of the electron density with position demands high momentum and therefore kinetic energy for the electrons, which can only be included using extensive plane-wave basis sets. By choosing a sufficiently large energy cutoff, DFT calculations performed using plane-wave basis sets can deliver highly reproducible results compared to alternate approaches such as the use of atomic basis sets [23]. In VASP, for each atom, a recommended cutoff kinetic-energy is available for each PP, with the cuffoff used in any calculation being the largest value required by any embodied atom. This recommended cutoff energy is designed to give useful results, but more reproducible results can be obtained if E_{cut} is increased. Recognizing this, the values of E_{cut} recommended for VASP's GW PPs are systematically increased compared to those for PBE PPs. In addition, in this work, we consider using either the default value for the PP, or else that increased by 30 %; such an increase is typical of specifications often used in high-quality calculations [23,29].

To perform the Brillouin zone integration in the three-dimensional reciprocal-lattice space, usually a discrete set of vectors, **k**, is chosen. There are several commonly used methods for selecting these vectors, which are known as "*k*-points". The method introduced by Baldereschi [30], extended by Chadi and Cohen [31], and further developed by Monkhorst and Pack [32], is the most widely used approach today, and we exclusively use this approach using Γ-centered meshes. In this approach, the crystallographic directions **a**, **b**, and **c** in reciprocal space are equally divided into N_a, N_b, and N_c regions, producing $N_a \times N_b \times N_c$ *k*-points at which the DFT wavefunctions need to be evaluated. The accuracy of the calculations of the total energy, and most other properties, of the material can be systematically improved by increasing the number of *k*-points used in the integration. From a practical perspective, however, the computational cost is usually linearly related to the number of irreducible *k*-points involved.

Generally applicable approaches for the automatic generation of *k*-point grids for materials have been developed by Wisesa et al. [33]. Using their simple-diagonal-grid approach, a maximum allowable separation in **k**-space between any two points is prescribed; this is known as the *k*-spacing, k_{sp}, from which the *k*-point grid is determined using

$$N_i = max\left(1, ceiling\left(|b_i| 2\pi / k_{sp}\right)\right)$$

In this equation, *i* represents one of the 3 crystallographic directions, $|b_i|$ is the length of the lattice vector in reciprocal space, and *ceiling*(*x*) is the ceiling function which returns the least integer that is equal or larger than *x*. In previous studies, $k_{sp} = 0.5$ Å^{-1} was determined to be a reasonable setting for most calculations [34], and this is currently the default value used by VASP. Nevertheless, setting k_{sp} too large can lead to significant errors, and, in this work, we consider calculations performed using values of $k_{sp} = 0.375$ Å^{-1}, as has been considered appropriate for crystal-structure geometry optimizations [35], and $k_{sp} = 0.22$ Å^{-1}, as has been considered appropriate, e.g., for GW calculations [36]. Nominally, computational cost scales as k_{sp}^3, but symmetry can minimize impact.

All observable properties of the material such as the total energy, atomic forces, and spectroscopic transition energies arise through the consideration of all *k*-points used, but useful approximations to electronic-spectroscopic transition energies and electrochemical potentials can, in principle, be obtained by considering only the orbital energies calculated at some critical *k*-points, negating the need for full integration over the Brillion zone, to deliver significant computational savings {Kim, 2020 #276}. In particular, the energy difference

$$\Delta E = E_{LUMO}(\mathbf{k}_{LUMO}) - E_{HOMO}(\mathbf{k}_{HOMO})$$

between the energy E_{HOMO} of the highest-occupied (HOMO) band maximum $\mathbf{k}_{HOMO}$ and that E_{LUMO} of the lowest-unoccupied band minimum $\mathbf{k}_{LUMO}$ is known as the *orbital bandgap* and provides a crude approximation to the lowest spectroscopic electronic transition energy as well as the difference between the energies needed to add or remove electronic charge. As determination of the orbital bandgap requires knowledge of the HOMO and LUMO orbitals, properties of the entire **k** space are relevant as the occupancies of *k*-point are globally determined. For semiconductors, the HOMO and LUMO are typically well-defined however, making ΔE simply a function of only $\mathbf{k}_{HOMO}$ and $\mathbf{k}_{LUMO}$. Alternatively, for metals, the orbital-band occupancies are difficult to determine reliably, and to induce stability the parameter $k_\beta T_E$ is usually introduced into the calculations, where T_E specifies a thermal temperature for the electrons and k_β is Boltzmann's constant [37]. Variations in the specification of $k_\beta T_E$ can modulate the nature of $\mathbf{k}_{HOMO}$ and $\mathbf{k}_{LUMO}$ and hence modulate the calculated bandgap. If $\mathbf{k}_{HOMO} = \mathbf{k}_{LUMO}$ then only one vector actually needs to be found, and the optical transition is refereed to as being *direct*; otherwise the transition is called *indirect*.

As each *k*-point represents a different symmetry, all *k*-point calculations are, in principle, independent of each other and so their properties can be determined in parallel on modern computer architectures. For GGA-type functionals such as PBE, modern computational strategies implement this principle. However, for hybrid functionals such as PBE0,

it is common in computational packages to expand the entire Hartree-Fock exchange energy about a critical vector in reciprocal space obtained by considering all k-points. The way that this is done in VASP, at least, embeds an unexpected dependence of the results at each k-point on the selection of the other k-points [38]. As a result, reliable orbital bandgaps can no longer be determined simply by evaluating the orbital energies at the two specific k-points specified by $\mathbf{k}_{HOMO}$ and $\mathbf{k}_{LUMO}$, as is done, e.g., in the construction of the bandgap database of Kim et al. [39].

In general, an important effect of variation of k_{sp} on the evaluation of bandgaps ΔE comes from how closely the points on the resulting k-point grids approach $\mathbf{k}_{HOMO}$ and $\mathbf{k}_{LUMO}$. In many cases, these vectors lie on high-symmetry points and can be easily anticipated, but this result is not guaranteed as, in principle, $\mathbf{k}_{HOMO}$ and $\mathbf{k}_{LUMO}$ could point in any direction. The distance from the closest point on some grid to the actual extremum points does not systematically improve as k_{sp} is made smaller. For example, if a direct transition occurs at the high-symmetry point $\mathbf{k} = \left(\frac{1}{2}, \frac{1}{2}, \frac{1}{2}\right)$, then using a small k-point mesh with $N_a = N_b = N_c = 2$ is sufficient to capture the HOMO and LUMO vectors at little computational cost. Indeed, any larger grid in which N_a, N_b, and N_c are all even will deliver the same results, but at proportionately greater computational expense. Nevertheless, if any of N_a, N_b, and N_c are odd, then no matter how large the grid is chosen to be, it will not include the extremum vectors and so the obtained results will not be "reproducible" if different users (of any code) enact small variations to the choice of the parameters N_a, N_b, and N_c.

For the choices of PP and energy cutoff E_{cut}, systematic procedures are available for enhancing the computational reproducibility, but this is not the case for the specification of the $\mathbf{k}$ integration parameters based upon k_{sp}. In this work, we present a scheme for optimizing N_a, N_b, and N_c that retain the useful features of k_{sp} for the optimization of energies, forces, and other properties, yet is also systematic in its ability to yield improved bandgaps ΔE.

The influence of the computational parameters such as PP, E_{cut}, and k_{sp} operate directly at every possible geometrical structure of a material. In addition, these parameters have an indirect effect in that they also modify the forces and hence the optimal structure predicted by each density functional. Optimizing the reliability of DFT calculations therefore also needs to consider the structure-property relationship for the material.

In summary, in this work, the sensitivity of calculated bandgaps is considered with respect to changes in the k-point mesh, E_{cut}, and PP as a function of materials structure. In total, nine sets of calculations are performed, named **a** – **i** in Fig. 1. These calculations are connected in the figure by arrows or lines, named **(i)** to **(x)**, that highlight single-parameter changes. Changes that are expected to lead to systematic improvements in the reproducibility of the calculations are marked with blue arrows, whereas unsystematic changes are marked with brown lines. For up to 340 selected materials evaluated using the PBE and PBE0 density functionals, calculated changes in the bandgap ΔE are then statistically analyzed, finding correlations of general use, as well as outliers and their origins.

2. Methods

2.1. Selection of 340 materials

We started considering the set of 472 3D materials that had been randomly selected by Borlido [40] from within the 2018 Materials-Project (MP) database [41]. Since then, the MP database has

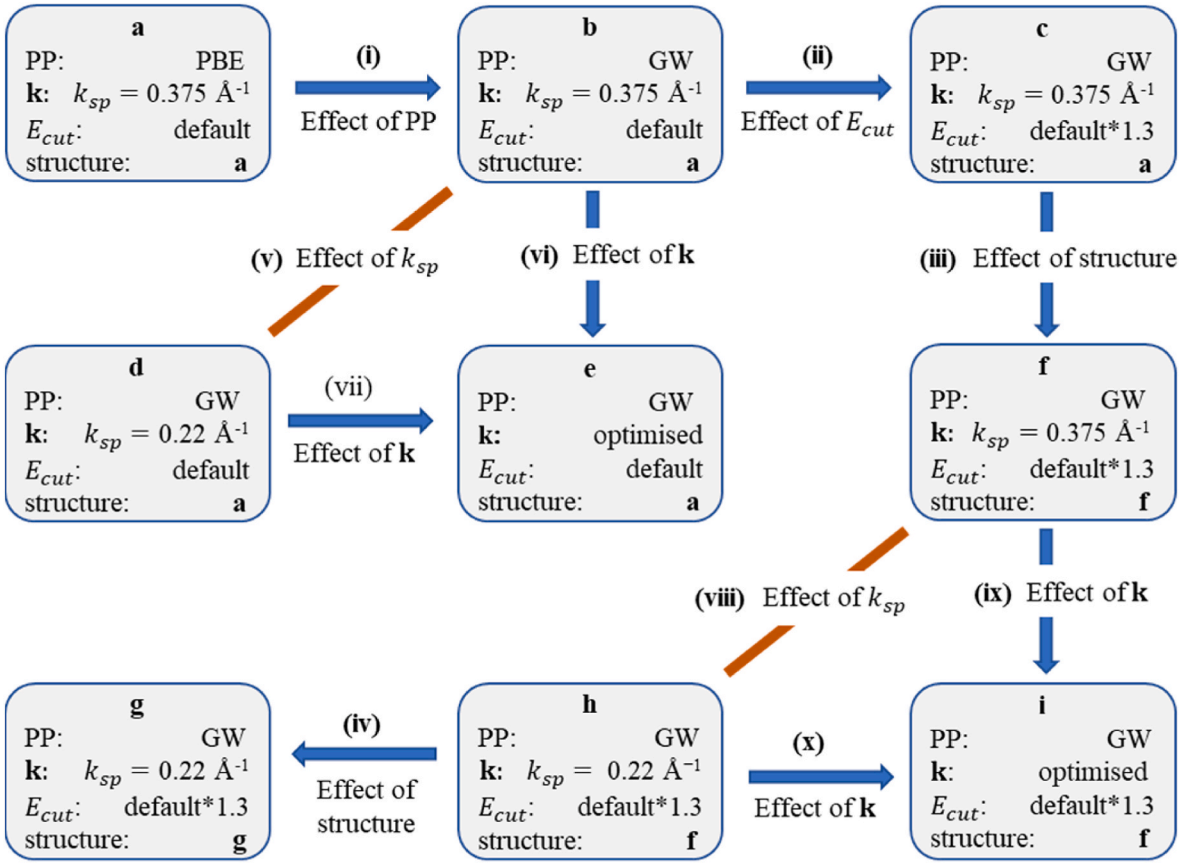

Fig. 1. Overview of the calculations performed, **a** – **i**, and single-step connections between them, **(i)**–**(x)**. Connections marked with blue arrows indicate systematic improvements, whereas brown connections do not. The structures used are those produced by structural optimizations performed in the stated calculations, either calculations **a**, **f**, or **g**.

been upgraded several times, with some of the 472 selected materials being significantly modified, with poor availability of the original structures. In addition, the modern MP database now lists primitive unit cells instead of the conventional ones accessed by Borlido et al. To avoid structural ambiguities, only structures preserved between the MP 2019 and 2022 databases are considered herin, utilizing the structure as represented in the 2022 MP database. Some of these materials were found to undergo significant structural changes when optimized using PBE, and these were also excluded from consideration. Finally, structures not computationally feasible for reproducible bandgap calculations using PBE0 owing to the computational resources required were also excluded. As a result, the number of materials considered was reduced to 340. Even still, not all PBE0 calculations were completed for this set, as detailed in Supplementary Material (SM).

2.2. General DFT procedures

The DFT computations were performed using VASP6.4.3. There are some significant computational parameters other than the three considered herein in detail. The computational algorithm, which in most cases was set to ALGO = ALL, but if this failed then ALGO = NORMAL was used. For PBE0, the results were found to be sensitive to the long-range treatment of the Hartree-Fock exchange component, with reproducible results only obtained using the default setting for HFRCUT. Other parameters included PREC = ACCURATE, an electronic loop convergence energy tolerance of 10^{-6} eV, and a geometry-optimization convergence criterion requiring the forces on each atom to be less than 10^{-3} eV Å^{-1}. The geometry optimizations were performed in 4 successive steps, optimizing in term all coordinates with the unit cell (ISIF = 2), the unit cell (ISIF = 6), all properties (ISIF = 3), and finally all atomic coordinates (ISIF = 2) again. All reported properties are obtained using subsequent single-point energy calculations. The wavefunction files were deleted between each computational step to remove memory effects.

2.3. A scheme to optimize the choice of k-point grids for bandgap calculations

To find a more robust method for determining $\mathbf{k}_{HOMO}$ and $\mathbf{k}_{LUMO}$, we utilise the computational efficiency of the PBE functional to perform calculations using a 16 × 16 × 16 k-points grid for each material. This grid-representation of the band energies was then interpolated to obtain the desired stationary points $\mathbf{k}_{HOMO}$ and $\mathbf{k}_{LUMO}$. For both the HOMO and LUMO, the Hessian matrices $\mathbf{H} = \frac{\partial E}{\partial \mathbf{k}^2}$ were determined numerically at the extremum grid points, as well as evaluating the associated first derivatives $\frac{\partial E}{\partial \mathbf{k}}$. The values of $\mathbf{k}_{HOMO}$ and $\mathbf{k}_{LUMO}$ were then obtained by interpolation, evaluating the differences $\Delta\mathbf{k}$ of the stationary points from the extremum grid points as

$$\Delta\mathbf{k} = -\mathbf{H}^{-1} \cdot \frac{\partial E}{\partial \mathbf{k}} .$$

Given $\mathbf{k}_{HOMO}$ and $\mathbf{k}_{LUMO}$, the task then becomes the determination of a k-point mesh that has grid points both sufficiently close to the desired vectors and extensive enough to allow related properties like spectroscopic transition energies to be evaluated. Such properties could be evaluated in subsequent works using e.g., ΔSCF, Green's function, or Bethe-Salpeter approaches. It is often assumed that k-point meshes produced by $k_{sp} = 0.375$ Å^{-1} are sufficient for such purpose, e.g., this being an improvement on the VASP default value of 0.5 Å^{-1}, but smaller values could be used if necessary. What is required then is a k-point mesh that is at least as large as the one indicated using k_{sp} yet has grid points close to both $\mathbf{k}_{HOMO}$ and $\mathbf{k}_{LUMO}$.

We consider every possible k-point mesh from that generated using $k_{sp} = 0.375$ Å^{-1} up to 16 × 16 × 16. For each possibility, the energy in the HOMO and LUMO band-extremum energies are estimated from the previously determined values of $\mathbf{k}_{HOMO}$ and $\mathbf{k}_{LUMO}$ and the Hessian matrix using

$$error = \frac{1}{2}\Delta\mathbf{k}\cdot\mathbf{H}\cdot\Delta\mathbf{k}$$

where now $\Delta\mathbf{k} = \mathbf{k}_{HOMO \text{ or } LUMO} - \mathbf{k}$ are the deviations from a grid point to the extremum values. If the estimated error in the bandgap is less than some threshold level ΔE_T which we choose to be 0.025 eV, then that k-points mesh is considered as a possible best choice. The best choice is obtained by determining which of the available options has the smallest k-points mesh in terms of the product $N_a \times N_b \times N_c$.

An alternative approach for finding the HOMO and LUMO vectors would be to perform calculations at all symmetry points, starting at high symmetry and proceeding towards some low-symmetry cutoff. This would have the disadvantage of not being able to guarantee that the correct result is obtained. Nevertheless, it would have the advantage over the interpolation approach in that high-symmetry values with, e.g., some k = 1/3, would be readily identified that are not included explicitly within the 16 × 16 × 16 grid. This is not a significant advantage, however, as the interpolation scheme would recognize the required value and hence the optimized grid would embody its nature. The interpolation scheme therefore delivers useful results to within the specified tolerance, without making any assumptions as to the relevance of high-symmetry points to the material of interest.

3. Results and discussion

Full details of the PBE and PBE0 results and their processing are provided in SM. This includes ASCII files listing the optimized coordinates of each material by each method plus some critical calculation parameters and results. Also included are Excel files listing 43 parameters or results for each of the 5526 completed calculations, along with their mathematical treatment that generates the results tables and figures, as well as the properties used in the optimization of the k-point grids and the anticipated resulting bandgap errors for each material.

Statistical summaries of the results from the 10 comparisons indicated in Fig. 1 are listed in Table 1. This includes the average deviations between the results (AVE), the mean-absolute deviations (MAD), the standard deviations (STDEV), and the minimum (MIN) and maximum (MAX) deviations. Low magnitudes are found for the AVE and MAD errors, with worst-case results of −0.10 eV and 0.15 eV, respectively. This indicates that, on average, computationally efficient schemes can deliver useful results. Nevertheless, the MIN and MAX deviations range from −2.77 eV to 0.95 eV, indicating that method changes can have profound consequences and hence computationally efficient schemes can deliver poor results. Subsequent analysis focuses mostly on unreliability, its causes, and the impact that similar effects could have on general DFT calculations. Table 2 highlights features of the most significant identified outliers.

3.1. Pseudopotential

The direct effect of the PP on calculated bandgaps is examined in comparison **(i)**. For it, Fig. 2 shows the correlations obtained for both PBE and PBE0 bandgaps calculated at the same geometry using the same E_{cut} and k_{sp}, considering the use of PBE versus GW PPs. Mostly, only small changes are found as a consequence of changing the PP, with Table 1 listing MAD changes of just 0.02 eV for PBE and 0.03 eV for PBE0. The largest changes found were 0.10 eV for PBE and 0.16 eV for PBE0, changes too small to be included in the outliers table, Table 2. Materials containing Ba were particularly sensitive to the quality of the PP, as was $Mo_2Sr_2O_8$ and AuCs.

Table 1
Statistical properties of the comparisons **(i)**–**(x)** shown in Fig. 1, including the average deviation (AVE), the mean absolute deviation (MAD), standard deviation (STDEV), and minimum (MIN) and maximum (MAX) deviations, all in eV, for up to 340 materials.

comparison	PBE					PBE0				
	AVE	MAD	STDEV	MIN	MAX	AVE	MAD	STDEV	MIN	MAX
(i) PP	−0.01	0.02	0.03	−0.07	0.10	0.01	0.03	0.04	−0.07	0.16
(ii) E_{cut}	0.00	0.00	0.01	−0.03	0.14	0.00	0.00	0.01	−0.04	0.04
(iii) structure[a]	−0.02	0.07	0.13	−1.16	0.50	−0.03	0.08	0.15	−1.16	0.52
(iv) structure	0.00	0.01	0.02	−0.16	0.13					
(v) k_{sp} [b]	−0.04	0.08	0.13	−1.26	0.70	−0.07	0.09	0.19	−1.75	0.95
(vi) k [c]	−0.07	0.10	0.16	−2.42	0.04	−0.08	0.12	0.25	−2.71	0.09
(vii) k [c]	−0.02	0.04	0.08	−1.16	0.11	−0.01	0.05	0.11	−1.21	0.23
(viii) k_{sp} [d]	−0.04	0.08	0.13	−1.39	0.70	−0.09	0.12	0.23	−1.71	0.73
(ix) k [e]	−0.07	0.10	0.16	−2.77	0.07	−0.10	0.15	0.28	−2.71	0.09
(x) k [f]	−0.03	0.04	0.08	−1.38	0.10	−0.02	0.07	0.15	−1.21	0.19

[a] 205 materials for PBE0.
[b] 339 materials for PBE0.
[c] 253 materials for PBE0.
[d] 178 materials for PBE0.
[e] 192 materials for PBE0.
[f] 170 materials for PBE0.

Table 2
Outliers in the comparisons **(i)** - **(iv)**, **(vi)**, **(vii)**, and **(ix)** – **(x)** (see Fig. 1), listing the calculated bandgaps ΔE (eV) and the changes between them (eV).[a]

Comp.	material	calc.	ΔE	calc.	ΔE	change
PBE						
(iii)	LiF	**c**	10.00	**f**	8.84	−1.16
	NaF	**c**	7.11	**f**	6.15	−0.97
	Mg2F4	**c**	7.52	**f**	6.84	−0.68
	CaF2	**c**	7.70	**f**	7.16	−0.54
	SrF2	**c**	7.27	**f**	6.83	−0.44
	Tl3AsSe3	**c**	1.16	**f**	0.74	−0.41
	RbF	**c**	5.92	**f**	5.52	−0.40
	Li2I2O6	**c**	3.30	**f**	3.81	0.50
(ix)	Bi4Cs6I18	**f**	2.32	**i**	2.40	0.07
(x)	KTaO3	**h**	2.16	**i**	2.26	0.10
PBE0						
(iii)	LiF	**c**	13.45	**f**	12.29	−1.16
	NaF	**c**	10.22	**f**	9.31	−0.91
	Mg2F4	**c**	10.80	**f**	10.17	−0.62
	CaF2	**c**	10.63	**f**	10.14	−0.49
	SrF2	**c**	10.21	**f**	9.74	−0.47
(vi)	Os2As4	**b**	2.04	**e**	2.13	0.09
(vii)	Fe2P4	**d**	2.27	**e**	2.50	0.23
	Os2As4	**d**	1.94	**e**	2.13	0.18
	KTaO3	**d**	4.32	**e**	4.45	0.13
	AuRb	**d**	0.78	**e**	0.90	0.12
	InP	**d**	1.88	**e**	1.98	0.10
	LiZnAs	**d**	2.10	**e**	2.19	0.10
(ix)	Os2As4	**f**	2.04	**i**	2.13	0.09
(x)	Os2As4	**h**	1.94	**i**	2.13	0.19
	KTaO3	**h**	4.32	**i**	4.45	0.13
	AuRb	**h**	0.82	**i**	0.94	0.12
	CdI2	**h**	4.05	**i**	4.16	0.11
	InP	**h**	2.03	**i**	2.12	0.10
	Sb2Te3	**h**	1.14	**i**	1.23	0.09

[a] For comparisons **(i)** - **(iv)**, outliers are shown of magnitude >0.4 eV, whereas, for comparisons **(vi)**, **(vii)**, **(ix)**, and **(x)**, all outliers are listed that are >0.09 eV. Comparisons **(v)** and **(vii)** are not listed the embodied changes are random in nature.

3.2. E_{cut}

Increasing the value of the plane-wave basis-set cutoff energy E_{cut} facilitates improved description of the electronic structure in close towards nuclei where electron densities can change quickly. Fig. 2 shows the correlations **(ii)** between sets of PBE or PBE0 band gaps calculated using the same PP, structure, and k_{sp}, using either the default value for E_{cut} or else this increased by 30 %. Akin to the results found for changing the PP, E_{cut} changes are found mostly have little effect, with MAD

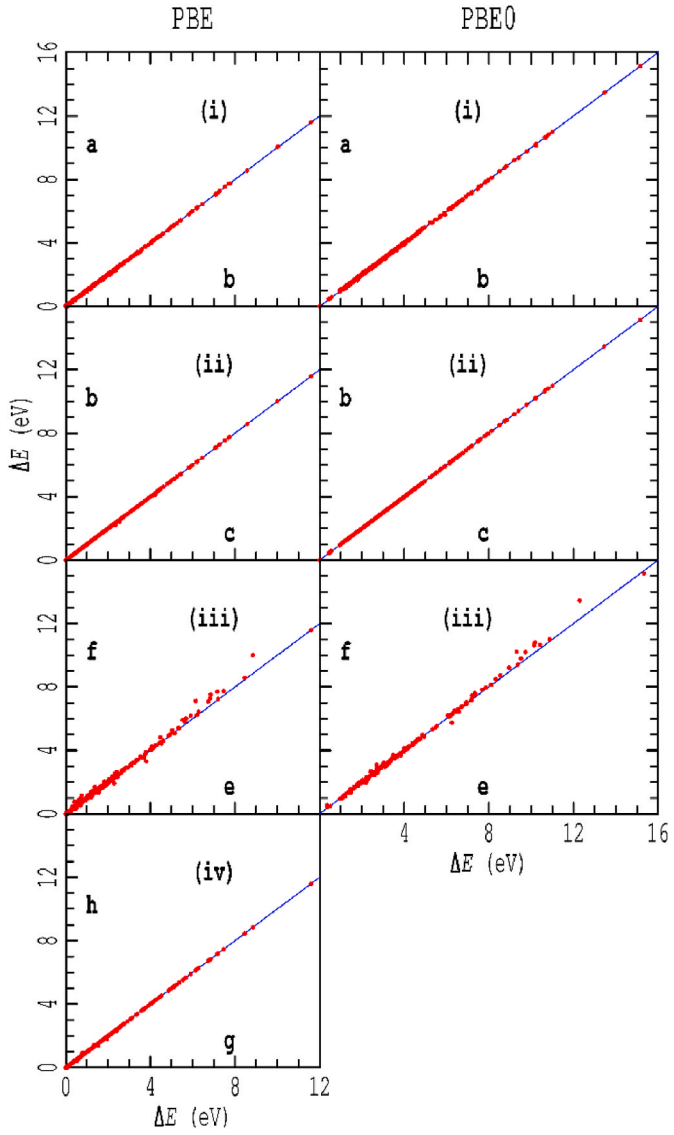

Fig. 2. Comparisons **(i)** to **(iv)** of calculation results **a**, **b**, **c**, **e**, **f**, **g**, and **h** (see Fig. 1), of bandgaps ΔE obtained using either the PBE or PBE0 density functional.

changes of <0.005 eV for both PBE and PBE0. The largest change obtained was 0.14 eV for the PBE calculation of $Bi_4Cs_6I_{18}$, but again this is too small to appear in Table 2.

3.3. Structural optimization

The comparisons **(iii)** and **(iv)** shown in Fig. 2 depict bandgap changes induced by geometry optimization. It is indeed common practice to use lower-cost approaches to optimize geometries and higher-cost approaches to evaluate properties based upon them, and these comparisons assess the reliability of this methodology. Computational parameters such as PP, E_{cut}, and k_{sp} not only have direct effects on bandgaps calculated at the same geometries but also can have indirect effects induced by geometry reoptimization. Specifically, comparison **(iii)** considers the indirect effect of both the PP and E_{cut}, whereas **(iv)** considers the computationally expensive effect of changing k_{sp} from 0.375 $Å^{-1}$ to 0.22 $Å^{-1}$ and is considered only using the PBE functional.

Statistical properties such as the MAD changes listed in Table 1 are small, being 0.07 eV using PBE and 0.08 eV using PBE0 for comparison **(iii)**, with just 0.01 eV using PBE for comparison **(iv)**. Nevertheless, the MIN and MAX changes can be large, from −1.16 eV to 0.52 eV for **(iii)**, reduced to between −0.16 eV and 0.13 eV for **(iv)**. The most significant outliers are listed in Table 2 and are often associated with fluorine chemistry, with the use of high quality PPs being required for accurate structural optimizations, as has previously been noted [23]. More broadly, significant errors exceeding the experimentally significant magnitude of 0.1 eV are found, 18 % and 21 % for PBE and PBE0 calculations for **(iii)** but just 1 % of PBE calculations for **(iv)**. In general, the use of crude PPS and low energy cutoffs in structural optimizations appears to be too risky to be used as a standard practice in modern calculations.

3.4. Brillouin-zone considerations

Fig. 3 shows results for each material for comparison sets **(v)** − **(x)**, obtained using either the PBE or PBE0 functionals. The presentation of the results is modified from that in Fig. 2 as now the differences between calculated bandgaps are shown as a function of what would naively be considered to be the poorer calculation. For example, for comparison **(v)**, the abscissa is the bandgap $\Delta E_{\mathbf{b}}$ from calculation series **b**, whereas the abscissa is the difference in bandgap from these results to those from series **d**, $\Delta E_{\mathbf{d}} - \Delta E_{\mathbf{b}}$. Negative differences correspond to the expectation that the better calculation delivers the lower bandgap, and attention focuses on the maximum magnitude of such negative differences, as well as the manifestation of any positive differences.

Comparisons **(v)**, and **(vii)**, marked in orange in Fig. 1, compare calculations performed using k_{sp} = 0.375 $Å^{-1}$ compared to 0.22 $Å^{-1}$. Each calculation interpolates the band energies on a grid, and naively the results from the finer grid are expected to provide a better approximation to the location of the valence and conduction band extrema. Indeed, using k_{sp} = 0.22 $Å^{-1}$ delivers results up to 1.6 eV lower than those from the courser k_{sp} = 0.375 $Å^{-1}$ grid, but the coarser grid could randomly describe the extrema better and is found to produce results that are up to 0.8 eV better. These random results are not highlighted in Table 2 as they are not considered to be outliers. Nevertheless, they serve to highlight the dangers in using any arbitrary scheme to search for the HOMO and LUMO extremum points in the Brillouin zone. For such an approach to be reproducible, the differences found when using different values of the arbitrary parameter (here k_{sp}) would need to be small, but the magnitude of the differences between the k_{sp} = 0.375 $Å^{-1}$ compared to 0.22 $Å^{-1}$ results is found to exceed the experimentally relevant bandgap change of 0.1 eV for 16 % of materials using PBE and for 23 % using PBE0. A higher percentage is expected for PBE0 than for PBE as the band structure is sharper for PBE0 owing to its larger bandgap, and hence inadequacies in **k** have a larger effect. The similarity

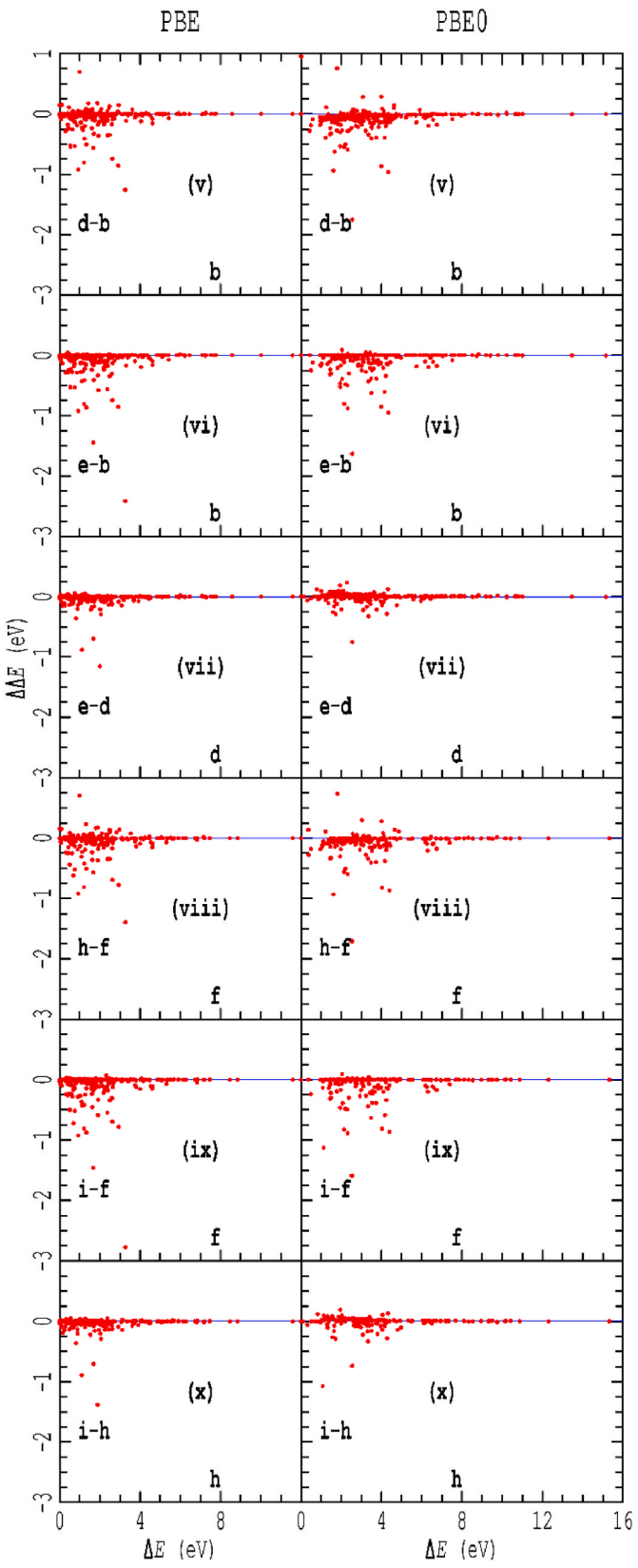

Fig. 3. Distribution diagrams of the bandgap differences $\Delta\Delta E$ for comparisons **(v)** to **(x)** versus the bandgap ΔE obtained from the more advanced method, involving calculation results **b**, **d**, **e**, **f**, **i**, and **h** (see Fig. 1), obtained using either the PBE or PBE0 density functional.

of the results presented in Fig. 3 for comparisons **(v)** and **(vii)** indicate that this effect is independent of other calculation properties, as expected.

Comparisons **(vi)**, **(vii)**, **(ix)** and **(x)** compare the results obtained using $k_{sp} = 0.375$ Å^{-1} or 0.22 Å^{-1} to those obtained using a grid optimized based upon the interpolation of PBE calculations using a 16 × 16 × 16 grid. The optimized grid is found to deliver bandgaps up to 2.5 eV lower than those obtained using an arbitrary grid. No results exceeding 0.05 eV, which is twice the error tolerance set in the grid-optimization procedure, are expected, and all results found exceeding 0.09 eV are listed in the outliers table, Table 2. Using PBE, only one such outlier is found from 1360 calculations, which could be expected based on random events. This indicates the effectiveness of the interpolation procedure.

Using PBE0, the situation is more complex, however. First, the integration grid that is used was optimized for PBE and then applied to PBE0, so if the band extrema occur at different values for PBE0, then the optimized grid may not include the actual extremum points.

Second, the numerical method used by VASP to determine the exchange energy for hybrid functionals involves the selection of a special value of the **k** vector, which is dependent on the entire **k**-point grid used [38], not just the properties of the extremum points. This occurs as the general expectation based on symmetry properties that the orbital energies obtained at one **k**-point are independent of the properties of any other **k**-point used in the calculation no longer holds. Hence this seemingly random effect could induce positive differences (as well as negative ones). For PBE0, only 1.6 % of the comparisons are reported as significant outliers in Table II, all of which can be attributed to one of these two issues. The optimized Brillouin-zone integration technique for hybrid functionals is therefore generally useful but not flawless.

4. Conclusions

The challenge of optimizing DFT calculation options to return reproducible bandgap predictions for a chosen functional was investigated considering four key parameters: the PP, the energy cutoff E_{cut}, the details of the geometry of the material, and the Brillouin-zone integration. Based upon analysis of calculations for up to 340 3D materials, the broad conclusion is that commonly applied protocols deliver useful results on average. Nevertheless, for a significant fraction of the calculations, significant shortcomings were identified, questioning the overall reproducibility of calculations performed using standard computationally efficient protocols.

Firstly, calculations of the bandgap using basic PPs and E_{cut} settings are found to provide excellent approximations for calculations done using the same structure, but when used to perform structural optimizations, these parameters led to significant errors in 18 % of cases for PBE and 21 % for PBE0. Their continued use in such commonly applied situations is therefore not recommended.

Secondly, automated schemes for determining the extremum HOMO and LUMO vectors for the estimation of orbital bandgaps, as well as optimizing integration grids for more general calculations, using k_{sp} are found to be inadequate as they suffer from large random errors that are experimentally significant for 16 % of the materials studied using PBE and 23 % using PBE0. To deliver reproducible results, a computational protocol was developed based on an interpolation scheme based upon PBE calculations for a 16 × 16 × 16 grid. This is found to work extremely well for PBE calculations, and to deliver results with only 1.6 % of materials manifesting experimentally significant errors when the PBE grid is applied in PBE0 calculations.

CRediT authorship contribution statement

Chenxi Lu: Writing – original draft, Investigation, Data curation. **Musen Li:** Supervision, Software, Methodology, Funding acquisition, Conceptualization, Investigation, Formal analysis, Writing – original draft. **Michael J. Ford:** Validation, Conceptualization, Formal analysis. **Rika Kobayashi:** Validation, Conceptualization, Formal analysis. **Roger D. Amos:** Validation, Investigation, Conceptualization, Formal analysis. **Jeffrey R. Reimers:** Writing – review & editing, Validation, Supervision, Investigation, Funding acquisition, Formal analysis, Data curation, Conceptualization.

Declaration of competing interest

The authors declare that they have no known competing financial interests or personal relationships that could have appeared to influence the work reported in this paper.

Acknowledgments

We thank the Young Scientists Fund of the National Natural Science Foundation of China (Grant No. 12404276), the Special Funds of the National Natural Science Foundation of China (Grant No. 12347164), the China Postdoctoral Science Foundation (Grant Nos. 2024T170541 and GZC20231535), the Australian Research Council Centre of Excellence in Quantum Biotechnology CE230100021, and National Computational Infrastructure (Australia) for provision of computing resources under NCMAS account d63 augmented by funding from the University of Technology Sydney, and also ANUMAS account ×89.

Appendix A. Supplementary data

Supplementary data to this article can be found online at https://doi.org/10.1016/j.cocom.2025.e01122.

References

[1] J.M. Rondinelli, E. Kioupakis, Annual review of materials research 45 (2015) 491.
[2] D. Golodnitsky, V. Yufit, M. Nathan, I. Shechtman, T. Ripenbein, E. Strauss, S. Menkin, E. Peled, J. Power Sources 153 (2006) 281.
[3] S. Sharma, K.K. Jain, A. Sharma, Mater. Sci. Appl. 6 (2015) 1145.
[4] P. Sharma, S. Pardeshi, R.K. Arora, M. Singh, Int. J. Emerg. Technol. Appl. Eng. 3 (2013) 113.
[5] K. Chopra, P. Paulson, V. Dutta, Prog. Photovoltaics Res. Appl. 12 (2004) 69.
[6] C.M. Davis, Opt. Eng. 24 (1985) 347.
[7] K.T.V. Grattan, T. Sun, Sensor Actuator Phys. 82 (2000) 40.
[8] K. Gupta, N. Gupta, K. Gupta, N. Gupta, Recent Advances in Semiconducting Materials and Devices, Springer, 2016.
[9] M.C. Scharber, N.S. Sariciftci, Adv. Mater. Technol. 6 (2021) 2000857.
[10] W. Kohn, L.J. Sham, Phys. Rev. 140 (1965). A1133.
[11] P. Hohenberg, W. Kohn, Phys. Rev. 136 (1964). B864.
[12] D. Golze, M. Dvorak, P. Rinke, Front. Chem. 7 (2019) 377.
[13] H.S. Yu, S.L. Li, D.G. Truhlar, J. Chem. Phys. 145 (2016) 130901.
[14] S. Kümmel, L. Kronik, Rev. Mod. Phys. 80 (2008) 3.
[15] A.D. Becke, J. Chem. Phys. 140 (2014) 18A301.
[16] J.P. Perdew, K. Burke, M. Ernzerhof, Phys. Rev. Lett. 77 (1996) 3865.
[17] C. Adamo, V. Barone, J. Chem. Phys. 110 (1999) 6158.
[18] J.P. Perdew, A. Zunger, Phys. Rev. B 23 (1981) 5048.
[19] K.-H. Xue, J.-H. Yuan, L.R.C. Fonseca, X.-S. Miao, Comput. Mater. Sci. 153 (2018) 493.
[20] A.I. Johnson, K.P.K. Withanage, K. Sharkas, Y. Yamamoto, T. Baruah, R.R. Zope, J. E. Peralta, K.A. Jackson, J. Chem. Phys. 151 (2019) 174106.
[21] D. Hait, M. Head-Gordon, J. Phys. Chem. Lett. 9 (2018) 6280.
[22] M. Li, R. Kobayashi, R.D. Amos, M.J. Ford, J.R. Reimers, Chem. Sci. 13 (2022) 1492.
[23] M. Li, J.R. Reimers, M.J. Ford, R. Kobayashi, R.D. Amos, J. Comput. Chem. 42 (2021) 1486.
[24] K. Lejaeghere, V. Van Speybroeck, G. Van Oost, S. Cottenier, Crit. Rev. Solid State Mater. Sci. 39 (2014) 1.
[25] F. Jollet, M. Torrent, N. Holzwarth, Computer Physics Communications, 185, 2014, p. 1246.
[26] G. Kresse, J. Hafner, Phys. Rev. B 47 (1993) 558.
[27] G. Kresse, J. Furthmüller, Comput. Mat. Sci. 6 (1996) 15.
[28] G. Kresse, D. Joubert, Phys. Rev. B 59 (1999) 1758.
[29] F. Aryasetiawan, O. Gunnarsson, Rep. Prog. Phys. 61 (1998) 237.
[30] A. Baldereschi, Phys. Rev. B 7 (1973), 5212.
[31] D.J. Chadi, M.L. Cohen, Phys. Rev. B 8 (1973), 5747.
[32] H.J. Monkhorst, J.D. Pack, Phys. Rev. B 13 (1976) 5188.
[33] P. Wisesa, K.A. McGill, T. Mueller, Phys. Rev. B 93 (2016) 155109.
[34] Q. Guo, G. Wang, E.R. Batista, K.C. Lau, P. Yang, ACS Appl. Nano Mater. 4 (2021) 5038.

[35] Z. Chen, H. Li, C. Zhang, H. Zhang, Y. Zhao, J. Cao, T. He, L. Xu, H. Xiao, Y. Li, H. Shao, X. Yang, X. He, G. Fang, J. Chem. Theor. Comput. 20 (2024) 9627.
[36] Y.-Y. Lv, Y. Zhou, L. Xu, Y. Luo, Y.-Y. Zhang, L. Cao, J. Zhou, Y.B. Chen, S.-H. Yao, S.-T. Zhang, Z. Yang, Y.-F. Chen, J. Phys. Condens. Matter 33 (2021) 105702.
[37] C. Jiang, Acta Mater. 56 (2008) 6224.
[38] I. Duchemin, F. Gygi, Comput. Phys. Commun. 181 (2010) 855.
[39] S. Kim, M. Lee, C. Hong, Y. Yoon, H. An, D. Lee, W. Jeong, D. Yoo, Y. Kang, Y. Youn, S. Han, Sci. Data. 7 (2020) 387.
[40] P. Borlido, T. Aull, A.W. Huran, F. Tran, M.A. Marques, S. Botti, J. Chem. Theor. Comput. 15 (2019) 5069.
[41] A. Jain, S.P. Ong, G. Hautier, W. Chen, W.D. Richards, S. Dacek, S. Cholia, D. Gunter, D. Skinner, G. Ceder, K.A. Persson, APL Mater. 1 (2013) 011002.